Research Square

Preprints are preliminary reports that have not undergone peer review.
They should not be considered conclusive, used to inform clinical practice,
or referenced by the media as validated information.

Individual and combined effects of sodium citrate and hydroxypropyl methylcellulose on floc structure and rheology of polycarboxylate ether-containing cement paste

Na Lian
Lanzhou University of Technology
Jiajia Wang
Lanzhou University of Technology
Rui Su
Lanzhou University of Technology
Yunsheng Zhang
zhangyunsheng2011@163.com
Lanzhou University of Technology
Yu Zhang
Lanzhou University of Technology
Jiufu Zhang
Lanzhou University of Technology
Hongxia Qiao
Lanzhou University of Technology

Research Article

Keywords: polycarboxylate ether, sodium citrate, hydroxypropyl methylcellulose, floc structure, rheology

Posted Date: November 17th, 2026

DOI: https://doi.org/10.21203/rs.3.rs-11278198/v1

License: This work is licensed under a Creative Commons Attribution 4.0 International License.
Read Full License

Additional Declarations: No competing interests reported.

Individual and combined effects of sodium citrate and hydroxypropyl methylcellulose on floc structure and rheology of polycarboxylate ether-containing cement paste

Na Lian [a, b], Jiajia Wang [a, b], Rui Su [a, b], Yunsheng Zhang [a, b, c*], Yu Zhang [a, b *], Jiufu Zhang [a, b], Hongxia Qiao [a, b]

[a] *School of Civil and Hydraulic Engineering, Lanzhou University of Technology, Lanzhou, Gansu, China*

[b] *Gansu Advanced Civil Engineering Materials Engineering Research Center, Lanzhou, Gansu 730050, China*

[c] *State Key Laboratory of Engineering Materials for Major Infrastructure, Southeast University, Nanjing 211189, China*

* Corresponding authors E-mail addresses:

zhangyunsheng2011@163.com (Yunsheng Zhang); yzhang20210036@163.com (Yu Zhang)

Abstract: Dispersion and thickening trends in single-admixture systems do not directly explain blended cement paste rheology, where interfacial state and floc structure change concurrently. At a water-to-cement ratio of 0.29, pastes containing polycarboxylate ether superplasticizer (PCE), sodium citrate (CA), and hydroxypropyl methylcellulose (HPMC) were prepared. PCE-only, binary, and ternary systems were characterized using rotational rheometry, optical imaging, apparent ζ-potential measurements, and total organic carbon (TOC) analysis. Increasing PCE dosage refined flocs and reduced flow resistance. CA produced a non-monotonic response: low-shear peak stress in the PCE-CA system decreased to 5.89 Pa at 0.10% CA and rose to 12.82 Pa at 0.20%. HPMC increased floc size and structural resistance. At 0.20% HPMC, low-shear peak stress and final apparent viscosity in the PCE-HPMC system reached 577.63 Pa and 9.9696 Pa·s, respectively. Both dosage-response trends persisted in the ternary systems, although their magnitudes depended on the coexisting admixture. Measured TOC values were lower than the sums from corresponding single-admixture systems, particularly in HPMC-containing mixtures. The absolute value of the apparent ζ potential correlated linearly with the two-dimensional projected fractal dimension, with R^2 values from 0.960 to 0.978. With increasing fractal dimension, dynamic yield stress and consistency index generally decreased, whereas the flow behavior index increased. These findings connect interfacial state, floc structure, and rheological response and support admixture formulation.

Keywords: polycarboxylate ether; sodium citrate; hydroxypropyl methylcellulose; floc structure; rheology

1 Introduction

Cement paste is a suspension comprising cement particles, early hydration products, and an aqueous phase. Its rheological behavior directly affects the transport, filling, and forming of fresh cement-based materials [1,2]. Pumping and casting require low flow resistance, whereas suppressing bleeding and segregation and retaining shape after placement require sufficient structural stability. Balancing these requirements involves controlling particle dispersion, flocculation, and structural rebuilding. During rest and shearing, particle contacts continually reorganize alongside the formation of early hydration products, making yield and viscous

responses dependent on time and shear conditions [3,4]. Chemical admixtures participate in these processes by modifying interparticle interactions and the aqueous environment. Their combined effects therefore depend on how the constituent admixtures jointly influence dispersion and structure formation.

Polycarboxylate ether superplasticizers (PCE) promote dispersion by adsorbing onto cement particles and early hydration products, with their side chains providing steric hindrance. Cement mineral composition and PCE charge characteristics affect adsorption behavior and dispersion efficiency [5,6]. Molecular topology and anionic charge density further influence their rheological effects [7,8]. The influence of PCE on structural build-up also involves interparticle interactions and early hydration kinetics [9,10]. Rheological control in PCE-containing pastes therefore involves surface adsorption, interparticle connections, and their evolution over time. Adding other admixtures alters the relationships among these processes.

Hydroxypropyl methylcellulose (HPMC) is a commonly used cellulose ether viscosity-modifying admixture. It regulates paste rheology through continuous-phase thickening and interactions between polymer chains and particles. Previous studies have shown that HPMC modifies the yield and viscous responses of PCE-containing pastes, with cellulose ethers influencing interparticle connections [11,12]. Studies of viscosity-modifying admixtures have also shown nonlinear structural build-up, with distinct evolution of static yield stress and storage modulus [13]. Studies of HPMC thickening mechanisms and chain length further show that polymer-chain characteristics affect particle bridging and paste flow resistance [14,15]. HPMC also influences early hydration, and its effects in the presence of PCE vary with binder composition [16,17]. These findings show that HPMC-induced thickening must be considered alongside particle structure and interfacial interactions to explain its influence on PCE dispersion.

Sodium citrate (CA) is used to regulate cement setting and paste workability, and its interaction with PCE provides another route for rheological control. Studies of citric acid have elucidated the role of citrate in early cement hydration [18]. Research on CA and PCE has shown that preferential citrate adsorption, delayed PCE adsorption, and aqueous calcium complexation jointly affect time-dependent rheology and viscoelastic behavior [19]. Sulfate carriers and cation composition further modify citrate-induced retardation, demonstrating the influence of the aqueous environment [20]. Competitive adsorption between superplasticizers and retarders, and between different polymers, also alters surface composition and paste rheology [21,22]. The effects of specialty admixtures coexisting with PCE on structural build-up have been investigated in the mortar phase of ultra-high-performance concrete [23]. When CA and HPMC coexist in PCE-containing paste, CA-induced changes in the aqueous and interfacial environments interact with HPMC-induced thickening and particle connections. Whether the dosage responses observed in binary systems persist in ternary systems is therefore a key question for admixture formulation.

Explaining these dosage responses requires linking changes in particle structure to macroscopic rheological behavior. Studies of cement paste structural build-up show that physical flocculation and hydration jointly contribute to the development of yield stress [24-26]. Particle packing, colloidal interactions, and hydration kinetics govern the specific processes of structural evolution [27]. Flocculation of weakly connected particles contributes to thixotropic recovery, while mixing conditions affect paste rheology by

altering floc formation and breakup [28,29]. Floc size and size distribution characterize particle aggregation and can be related to flow resistance [30]. Optical imaging and fractal analysis further quantify particle organization and floc geometry, enabling structural differences among mixtures to be compared with time-dependent fluidity and rheological parameters [31,32]. Floc size and geometry therefore provide important structural information for understanding how admixture effects translate into macroscopic rheological responses.

Particle interfacial state provides an additional basis for interpreting changes in floc structure. Polymer adsorption modifies the ζ potential and particle organization of cement minerals and hydration products [33]. Aqueous-phase speciation also affects the electrokinetic response of particle surfaces [34]. Pore solution composition and superplasticizers can alter interparticle forces and rheology, as demonstrated in metakaolin suspensions [35]. Broader studies have also linked ζ potential to the fresh-state behavior of cementitious materials [36]. Recent research has linked yield-stress changes caused by competitive adsorption between viscosity-modifying admixtures and PCE to interparticle forces and the network percolation threshold [37]. This connection highlights the combined roles of interfacial interactions and particle-network connectivity in macroscopic rheology. Existing studies have established relationships among admixture adsorption, particle structure, and rheological behavior. For ternary PCE-CA-HPMC systems, however, how CA and HPMC coexistence modifies their respective dosage responses remains to be clarified. The corresponding changes in interfacial electrokinetic state, floc geometry, and rheological parameters require direct comparison between binary and ternary systems.

This study investigated cement pastes at a water-to-cement ratio of 0.29 using PCE-only, binary PCE-CA and PCE-HPMC, and ternary PCE-CA-HPMC systems. In the ternary systems, either the CA or HPMC dosage was fixed while the other was varied to compare their individual and combined dosage responses. Rotational rheometry and optical image analysis after standardized dilution characterized yield and viscous responses, floc size, and two-dimensional projected fractal characteristics. Apparent ζ-potential measurements and total organic carbon analysis characterized the interfacial electrokinetic state and changes in residual organic carbon in the aqueous phase. Relationships among these measurements were examined to clarify how CA and HPMC coexistence affects floc structure and rheological behavior in PCE-containing pastes. The study provides a basis for selecting admixture combinations and dosages.

2 Materials and methods

2.1 Materials

P·O 42.5 ordinary Portland cement produced by Qilianshan Cement Co., Ltd. was used in this study. The cement had a specific surface area of 349 m²/kg, initial and final setting times of 168 and 227 min, respectively, and a 28 d compressive strength of 48.2 MPa. Its chemical composition is listed in Table 1, and the particle size and cumulative particle size distributions are shown in Fig. 1.

Polycarboxylate ether (PCE) superplasticizer, hydroxypropyl methylcellulose (HPMC), and sodium citrate (CA) were used as

chemical admixtures. The PCE was supplied by Jiangsu Sobute New Materials Co., Ltd. and had a water-reduction rate of 30.1%. HPMC was supplied by Linyi Yiqun Chemical Co., Ltd. as a powdered viscosity-modifying admixture with a nominal viscosity of 200,000 mPa·s. CA was supplied by Weike Building Materials Sales Center as a powdered retarder with a purity of not less than 99%. The basic properties of PCE, HPMC, and CA are summarized in Tables 2-4, respectively. Tap water was used for preparing all cement pastes.

Table 1. Chemical composition of Qilianshan P·O 42.5 cement (%).

CaO	SiO_2	Al_2O_3	Fe_2O_3	MgO	SO_3	Others
51.68	26.77	10.63	3.70	1.74	3.23	2.25

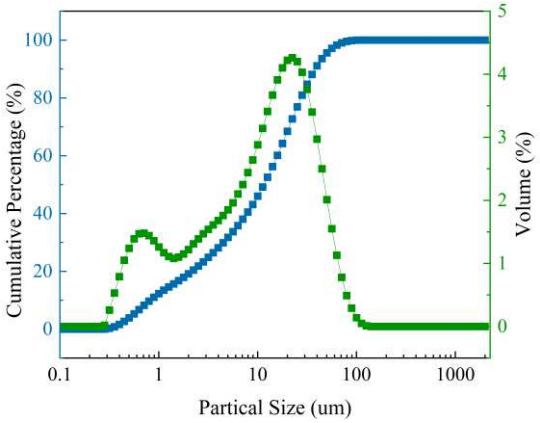


Fig. 1. Particle size distribution and cumulative distribution of Qilianshan P·O 42.5 cement.

Table 2. Basic properties of PCE.

Cl- (%)	Alkali content (%)	Water-reduction rate (%)	pH value	Solid content (%)
0.03	3.75	30.1	7.0	40.0

Table 3. Basic properties of HPMC.

Viscosity (mPa·s)	MS (Methyl)	MS (Hydroxypropyl)
200000	1.8-2.0	0.2-0.3

Table 4. Basic properties of CA.

pH	N (%)	Cl (%)	SO_4 (%)	PO_4 (%)	Other substances (%)	Solid content (%)
7.5-9.0	≤0.001	≤0.001	≤0.005	≤0.002	≤0.006	99

2.2 Mix proportions and paste preparation

The water-to-cement ratio of all cement pastes was fixed at 0.29, and the admixture dosages were expressed as percentages by mass of cement. Five series were investigated, namely PCE, PCE-CA, PCE-HPMC, PCE-HPMC-CA, and PCE-CA-HPMC, as detailed in Table 5.

For the PCE series, the PCE dosage was varied from 0 to 1.20% at levels of 0, 0.30%, 0.60%, 0.90%, and 1.20%. For the PCE-CA and PCE-HPMC series, the PCE dosage was fixed at 0.60%, while the CA and HPMC dosages were varied, respectively. In the

PCE-HPMC-CA series, the PCE and HPMC dosages were fixed at 0.60% and 0.10%, respectively, while the CA dosage was varied from 0 to 0.20%. In the PCE-CA-HPMC series, the PCE and CA dosages were fixed at 0.60% and 0.10%, respectively, while the HPMC dosage was varied from 0 to 0.20%. The numerical suffix in each sample designation represents the dosage of the variable admixture in the corresponding series.

Table 5. Mix proportions.

SampleID	Water/Cement	PCE(%)	CA(%)	HPMC(%)
PCE0	0.29	0	0	0
PCE0.30	0.29	0.30	0	0
PCE0.60	0.29	0.60	0	0
PCE0.90	0.29	0.90	0	0
PCE1.20	0.29	1.20	0	0
P-CA0	0.29	0.60	0	0
P-CA0.05	0.29	0.60	0.05	0
P-CA0.10	0.29	0.60	0.10	0
P-CA0.15	0.29	0.60	0.15	0
P-CA0.20	0.29	0.60	0.20	0
P-HPMC0	0.29	0.60	0	0
P-HPMC0.05	0.29	0.60	0	0.05
P-HPMC0.10	0.29	0.60	0	0.10
P-HPMC0.15	0.29	0.60	0	0.15
P-HPMC0.20	0.29	0.60	0	0.20
P-HPMC-CA0	0.29	0.60	0	0.10
P-HPMC-CA0.05	0.29	0.60	0.05	0.10
P-HPMC-CA0.10	0.29	0.60	0.10	0.10
P-HPMC-CA0.15	0.29	0.60	0.15	0.10
P-HPMC-CA0.20	0.29	0.60	0.20	0.10
P-CA-HPMC0	0.29	0.60	0.10	0
P-CA-HPMC0.05	0.29	0.60	0.10	0.05
P-CA-HPMC0.10	0.29	0.60	0.10	0.10
P-CA-HPMC0.15	0.29	0.60	0.10	0.15
P-CA-HPMC0.20	0.29	0.60	0.10	0.20

All cement pastes were prepared using an NJ-160B cement paste mixer. The cement, mixing water, and prescribed admixtures were introduced into the mixing bowl and mixed at low speed for 120 s. After a 15 s pause, the paste was mixed at high speed for a further 120 s. The same mixing procedure was used for all mixtures.

2.3 Test methods

2.3.1 Rheological measurements

The rheological properties of the cement pastes were measured using an AMETEK Brookfield RSX rotational rheometer. For each test, 50 mL of freshly mixed cement paste was placed in the rheometer sample cup and tested according to a predefined shear protocol.

The test consisted of two stages: low-shear constant-rate shearing and dynamic shearing. First, the paste was sheared at a constant shear rate of 0.1 s^{-1} for 60 s, during which the evolution of shear stress with time was continuously recorded. The maximum shear stress measured during this stage was defined as the low-shear peak stress, τ_s. The shear rate was then linearly increased from 0 to 100 s^{-1} over 75 s and subsequently decreased from 100 to 0 s^{-1} over another 75 s. The corresponding shear stress and apparent viscosity were recorded throughout the procedure.

The descending branch of the shear stress-shear rate curve was fitted using the Herschel-Bulkley model:

$$\tau = \tau_0 + K\gamma^n \tag{1}$$

where τ is the shear stress, τ_0 is the dynamic yield stress, K is the consistency index, γ is the shear rate, and n is the flow behavior index.

The apparent viscosity was calculated as:

$$\eta = \frac{\tau}{\gamma} \tag{2}$$

where η is the apparent viscosity. The apparent viscosity at a shear rate of 100s^{-1} was defined as the final apparent viscosity, η_f.

2.3.2 Microscopic imaging and analysis of floc structure

Floc morphology was examined using a DMM-900C optical microscope. All cement pastes underwent a standardized dilution procedure before imaging to reduce overlap among particles in the two-dimensional projections.

Fresh cement pastes were prepared according to the mix proportions in Table 5. A small amount of paste was transferred into a container and diluted with distilled water at 100 times the paste volume. The suspension was stirred for 10 s at a constant rate. Immediately after stirring, a sample was collected from the middle portion of the suspension and prepared for microscopic observation. Images were acquired promptly using the automated scanning mode to minimize the influence of particle sedimentation. The dilution ratio, stirring duration, sampling position, and image-acquisition conditions were identical for all mixtures.

All images were processed using the same segmentation procedure to identify the two-dimensional projected regions of the flocs. Mean chord length was used to characterize mean floc size, and the projected area fractions of flocs in different size ranges were determined. The two-dimensional projected fractal dimension, D_f, was calculated based on planar fractal theory. Fig. 2 illustrates

the specimen preparation and image-analysis procedure.

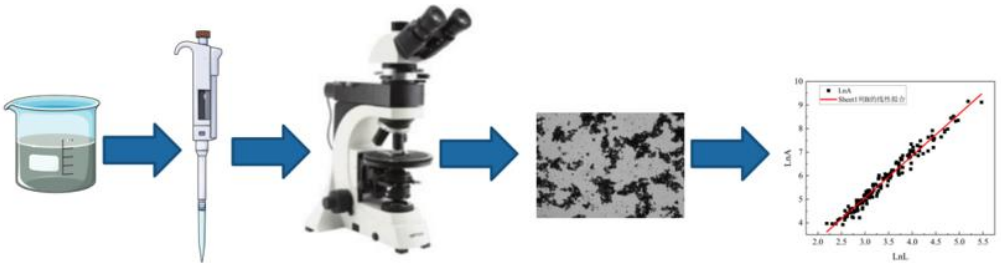


Fig. 2. Flowchart of floc-structure analysis.

2.3.3 Apparent ζ-potential measurement

The apparent ζ potential of cement particles was measured using a Zetasizer Nano ZS analyzer. According to the admixture composition of each test series, 20 mL of single-admixture or blended-admixture aqueous solution was prepared and mixed with 1 g of cement by manual stirring for 5 min, followed by 1 min of standing. Subsequently, 1.0 g of the upper suspension was collected and diluted with 49 g of deionized water for immediate measurement. The entire procedure, from the addition of cement to completion of the ζ-potential measurement, was controlled within 10 min. Each sample was tested in triplicate.

2.3.4 TOC analysis

Total organic carbon (TOC) analysis was used to determine the residual organic-carbon content in the supernatant after contact between cement and admixture solutions. Single-admixture solutions of PCE, CA, and HPMC at concentrations ranging from 0 to 2.0 g/L were prepared, and their TOC contents were measured to establish calibration relationships between admixture concentration and TOC content.

For each test, 20 mL of admixture solution was mixed with 1 g of cement by manual stirring for 5 min. The suspension was centrifuged at 4000 r/min for 5 min, and the supernatant was collected and filtered. The filtrate was diluted to a suitable concentration and analyzed using a TOC analyzer. For the single-admixture systems, the residual admixture concentration was determined from the corresponding calibration relationship.

The blended-admixture systems were tested using the same preparation and measurement procedures. The measured TOC value was obtained directly from the supernatant of each blended system. An additive baseline was calculated by summing the supernatant TOC contents of the corresponding single-admixture systems at the same concentrations. The deviation of the measured value from this baseline was used to characterize the non-additive response of residual organic carbon in the aqueous phase when multiple admixtures coexisted.

3 Results and discussion

3.1 Rheological properties of cement pastes with different admixture systems

Fig. 3 presents the rheological responses of the five admixture systems. The low-shear stress responses are shown in Figs. 3(a), (c), (e), (g), and (i), while the corresponding flow and apparent-viscosity curves are shown in Figs. 3(b), (d), (f), (h), and (j). The descending branches of the flow curves were fitted using the Herschel-Bulkley model, and the resulting parameters are summarized

in Table 6.

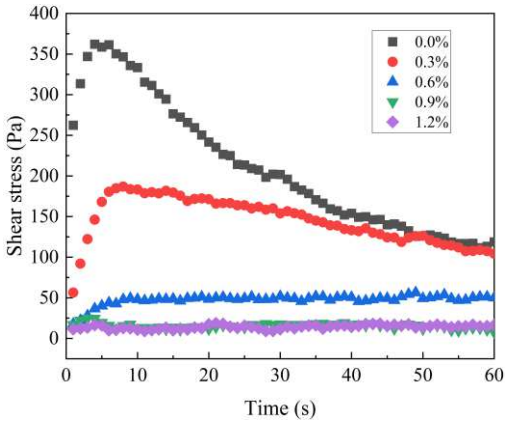
Increasing PCE dosage reduced the low-shear peak stress and apparent viscosity. As the dosage increased from 0 to 1.20%, the low-shear peak stress, τ_s, decreased from 362.01 to 21.15 Pa, and the fitted dynamic yield stress, τ_0, decreased from 75.09 to 0 Pa. The final apparent viscosity, η_f, decreased from 2.8542 to 0.5312 Pa·s. Meanwhile, the fitted flow behavior index, n, increased from 0.7819 to 1.8280, indicating a transition from shear-thinning to shear-thickening behavior. These results show that PCE reduced flow resistance under both low-shear conditions and at a shear rate of 100 s^{-1}.

CA produced different dosage responses in low-shear peak stress and final apparent viscosity. At a fixed PCE dosage of 0.60%, adding 0.05% CA reduced τ_s from 60.05 to 17.68 Pa, and increasing the CA dosage to 0.10% further reduced τ_s to 5.89 Pa. At this dosage, τ_0 was 0 Pa and the consistency index, K, was 0.018 Pa·s^n. Further increasing CA to 0.20% raised τ_s to 12.82 Pa. In contrast, η_f decreased from 1.1743 Pa·s at 0.05% CA to 0.8161 Pa·s at 0.20% CA. Thus, the dosage giving the lowest low-shear peak stress differed from that giving the lowest viscosity at 100 s^{-1}.

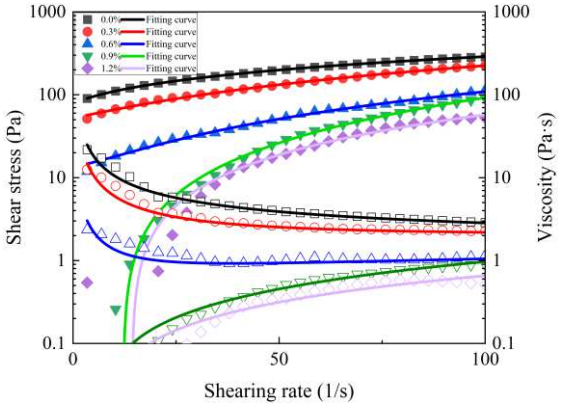
HPMC increased the low-shear peak stress and viscous resistance of PCE-containing paste. As the HPMC dosage increased from 0.05% to 0.20%, τ_s increased from 81.05 to 577.63 Pa and τ_0 increased from 13.08 to 357.96 Pa. Over the same range, K increased from 4.737 to 29.194 Pa·s^n, while n decreased from 0.9634 to 0.6729, indicating more pronounced shear thinning. At 0.20% HPMC, η_f reached 9.9696 Pa·s, compared with 1.1337 Pa·s for PCE0.60. The concurrent increases in τ_s, τ_0, and η_f show that HPMC raised resistance to flow under both low and high shear.

With PCE and HPMC fixed at 0.60% and 0.10%, respectively, CA retained its non-monotonic effect on the low-shear peak stress. Adding 0.05% and 0.10% CA reduced τ_s from 283.26 Pa to 71.66 and 38.17 Pa, respectively. Further increasing CA to 0.20% raised τ_s to 90.40 Pa. The viscosity response had a different turning point: η_f decreased from 8.1226 Pa·s at 0.05% CA to 6.3946 Pa·s at 0.15% CA, then increased to 7.0966 Pa·s at 0.20% CA. As in the binary PCE-CA system, the low-shear peak stress and viscosity at 100 s^{-1} did not reach their minima at the same CA dosage.

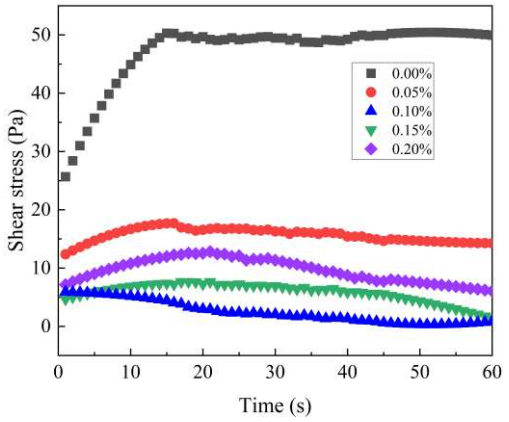
With PCE and CA fixed at 0.60% and 0.10%, respectively, increasing HPMC dosage raised both yield resistance and final apparent viscosity. As HPMC increased from 0 to 0.20%, τ_s increased from 5.89 to 382.79 Pa, τ_0 increased from 0 to 325.71 Pa, and η_f increased from 1.0875 to 8.3046 Pa·s. Between 0.15% and 0.20% HPMC, K increased from 66.905 to 325.708 Pa·s^n and n decreased from 0.4018 to 0.1507. The high-dose increase in K therefore accompanied a stronger shear-thinning response and higher yield resistance. These results show that HPMC continued to increase flow resistance in the presence of both PCE and CA.


Shear stress (Pa)
Time (s)
0.0%
0.3%
0.6%
0.9%
1.2%

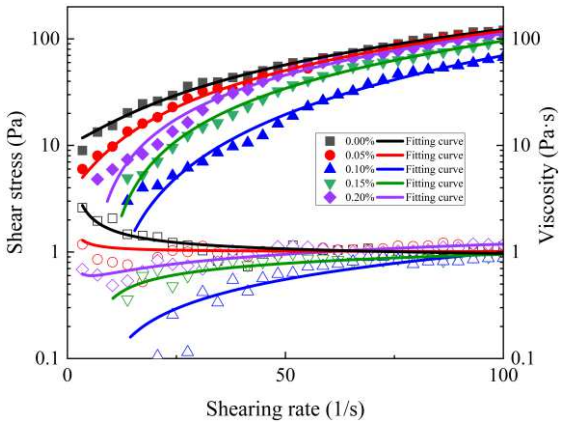
(a)


Shear stress (Pa)
Viscosity (Pa·s)
Shearing rate (1/s)
Fitting curve

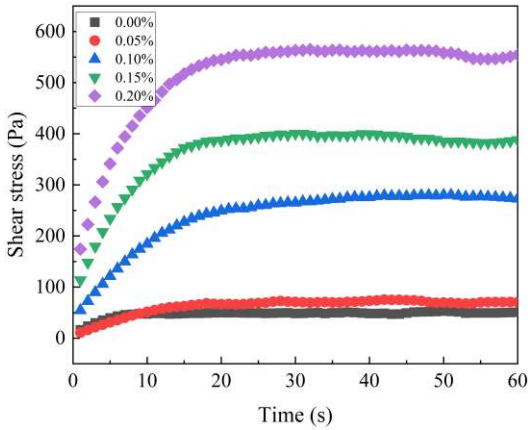
(b)


Shear stress (Pa)
Time (s)
0.00%
0.05%
0.10%
0.15%
0.20%

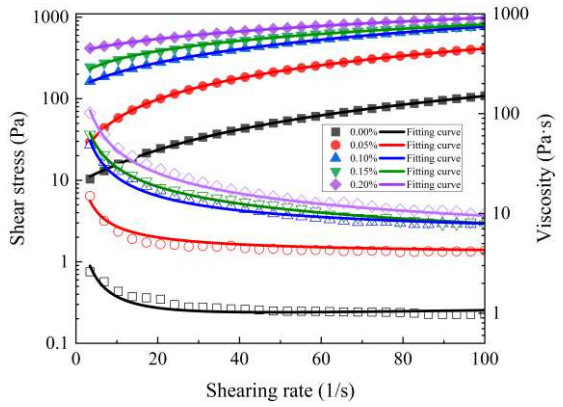
(c)


Shear stress (Pa)
Viscosity (Pa·s)
Shearing rate (1/s)
Fitting curve

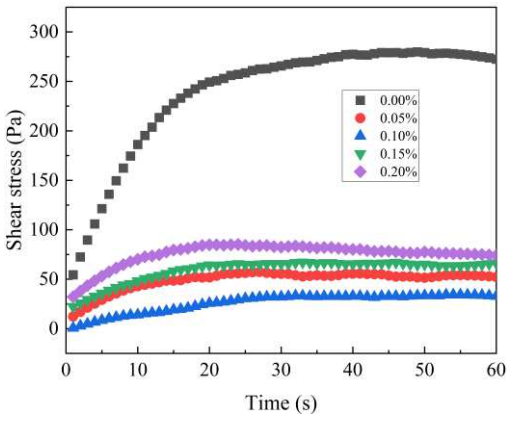
(d)


Shear stress (Pa)
Time (s)
0.00%
0.05%
0.10%
0.15%
0.20%

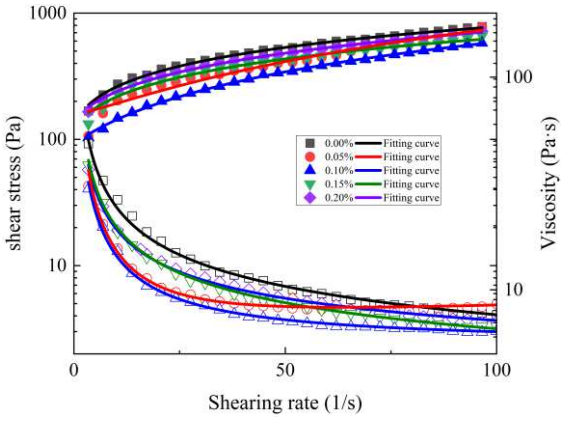
(e)


Shear stress (Pa)
Viscosity (Pa·s)
Shearing rate (1/s)
Fitting curve

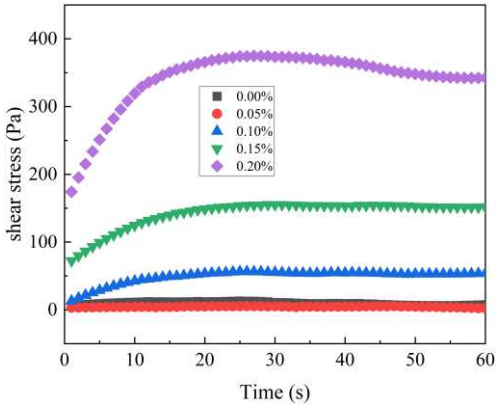
(f)


Shear stress (Pa)
Time (s)
0.00%
0.05%
0.10%
0.15%
0.20%

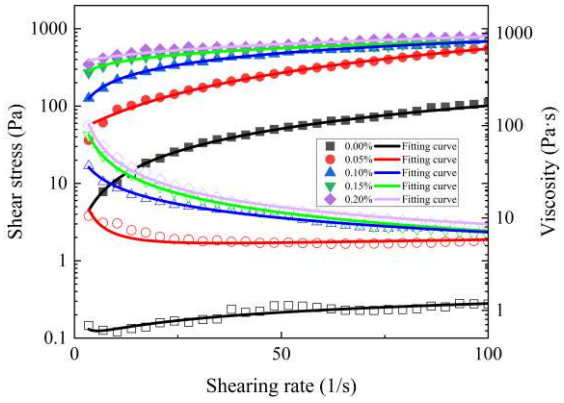
(g)


shear stress (Pa)
Viscosity (Pa·s)
Shearing rate (1/s)
Fitting curve

(h)



(i)



(j)

Fig. 3. Low-shear stress responses (a, c, e, g, and i) and flow and apparent-viscosity curves (b, d, f, h, and j) of the PCE, PCE-CA, PCE-HPMC, PCE-HPMC-CA, and PCE-CA-HPMC systems, respectively.

194 Table 6. Rheological parameters of cement pastes containing different admixture combinations.

Sample	τ_s (Pa)	τ_0 (Pa)	K (Pa·s^n)	n	R^2	η_f (Pa·s)
PCE0	362.01	75.09	5.822	0.7819	0.9997	2.8542
PCE0.30	186.01	52.84	1.011	1.1153	0.9983	2.2185
PCE0.60	60.05	13.70	0.23	1.3129	0.9959	1.1337
PCE0.90	29.27	0.00	0.021	1.4596	0.9986	0.9152
PCE1.20	21.15	0.00	0.076	1.8280	0.9909	0.5312
P-CA0.05	17.68	3.49	0.328	1.2854	0.9903	1.1743
P-CA0.10	5.89	0.00	0.018	1.7944	0.9978	1.0875
P-CA0.15	7.66	0.00	0.152	1.4058	0.9979	0.8722
P-CA0.20	12.82	1.26	0.308	1.2387	0.9946	0.8161
P-HPMC0.05	81.05	13.08	4.737	0.9634	0.9999	4.2333
P-HPMC0.10	283.26	131.87	9.130	0.9219	0.9999	8.1226
P-HPMC0.15	410.89	164.64	18.785	0.7616	0.9986	7.8113
P-HPMC0.20	577.63	357.96	29.194	0.6729	0.9994	9.9696
P-HPMC-CA0.05	71.66	127.64	5.131	0.9939	0.9949	8.1226
P-HPMC-CA0.10	38.17	111.06	5.406	1.0693	0.9871	6.7342
P-HPMC-CA0.15	65.04	133.99	21.334	0.6941	0.9861	6.3946
P-HPMC-CA0.20	90.40	134.16	26.406	0.7528	0.9938	7.0966
P-CA-HPMC0.05	18.76	37.53	2.074	0.5959	0.9976	5.6003
P-CA-HPMC0.10	38.17	111.06	5.406	1.0693	0.9871	6.7342

P-CA-HPMC0.15	161.88	148.79	66.905	0.4018	0.9730	7.5966
P-CA-HPMC0.20	382.79	325.71	325.708	0.1507	0.9652	8.3046

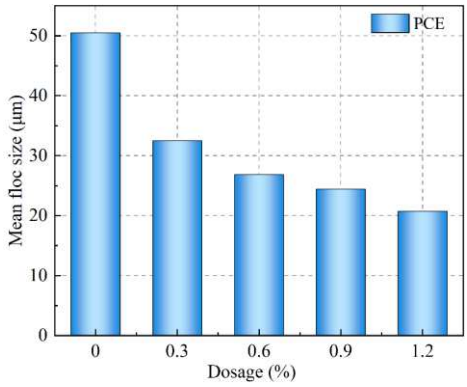
3.2 Floc structure characteristics of cement pastes with different admixture systems

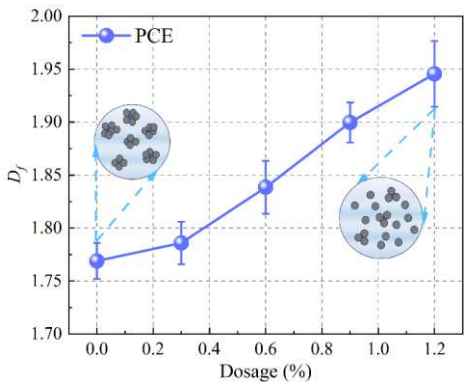
Fig. 4 shows the variations in mean floc size and two-dimensional projected fractal dimension, D_f, for the different admixture systems, while Fig. 5 presents the projected area fractions of flocs within different size ranges. Based on the mean chord length, the flocs were classified into five size ranges: ES (1-5 μm), S (5-25 μm), M (25-60 μm), L (60-95 μm), and EL (95-1000 μm).

For the PCE-only system, increasing the PCE dosage from 0 to 1.20% continuously reduced the mean floc size while increasing D_f, as shown in Figs. 4(a) and (b). As shown in Fig. 5(a), the combined area fraction of ES and S flocs increased from 6.98% to 18.26%, whereas that of M and L flocs decreased from 16.50% to 1.44%. These changes indicate progressive breakup of larger flocs and a shift in the floc size distribution toward smaller size ranges. Over the same dosage range, the low-shear peak stress decreased from 362.01 to 21.15 Pa, showing good consistency between floc refinement and the reduction in yield resistance.

The PCE-CA system exhibited a pronounced dosage-dependent response. As the CA dosage increased to 0.10%, the mean floc size decreased while D_f increased; further addition of CA reversed both trends, as shown in Figs. 4(c) and (d). At 0.10% CA, Fig. 5(b) shows that the combined area fraction of ES and S flocs increased from 11.60% to 12.82%, while that of M, L, and EL flocs decreased from 8.09% to 5.01%. When the CA dosage was further increased to 0.20%, the ES and S fraction decreased to 7.65%, whereas the combined M, L, and EL fraction increased to 13.09%. The low-shear peak stress correspondingly increased from its minimum value of 5.89 Pa to 12.82 Pa. Thus, the floc structure was most refined at approximately 0.10% CA, whereas further CA addition promoted the reformation of flocs in the M, L, and EL size ranges, accompanied by a recovery of low-shear resistance.

The PCE-HPMC system showed a distinctly different structural evolution. Increasing the HPMC dosage continuously increased the mean floc size and reduced D_f, as shown in Figs. 4(c) and (d). Fig. 5(c) shows that the combined area fraction of ES and S flocs decreased from 11.59% to 5.07%, whereas that of M, L, and EL flocs increased from 8.09% to 18.94%. The floc size distribution therefore shifted progressively toward medium and large size ranges. By increasing the viscosity of the continuous phase, HPMC facilitates the formation of larger structural units from smaller flocs, while polymer-chain interactions may further strengthen interparticle connections. Consistently, the low-shear peak stress increased from 60.05 Pa for PCE0.60 to 577.63 Pa for P-HPMC0.20.





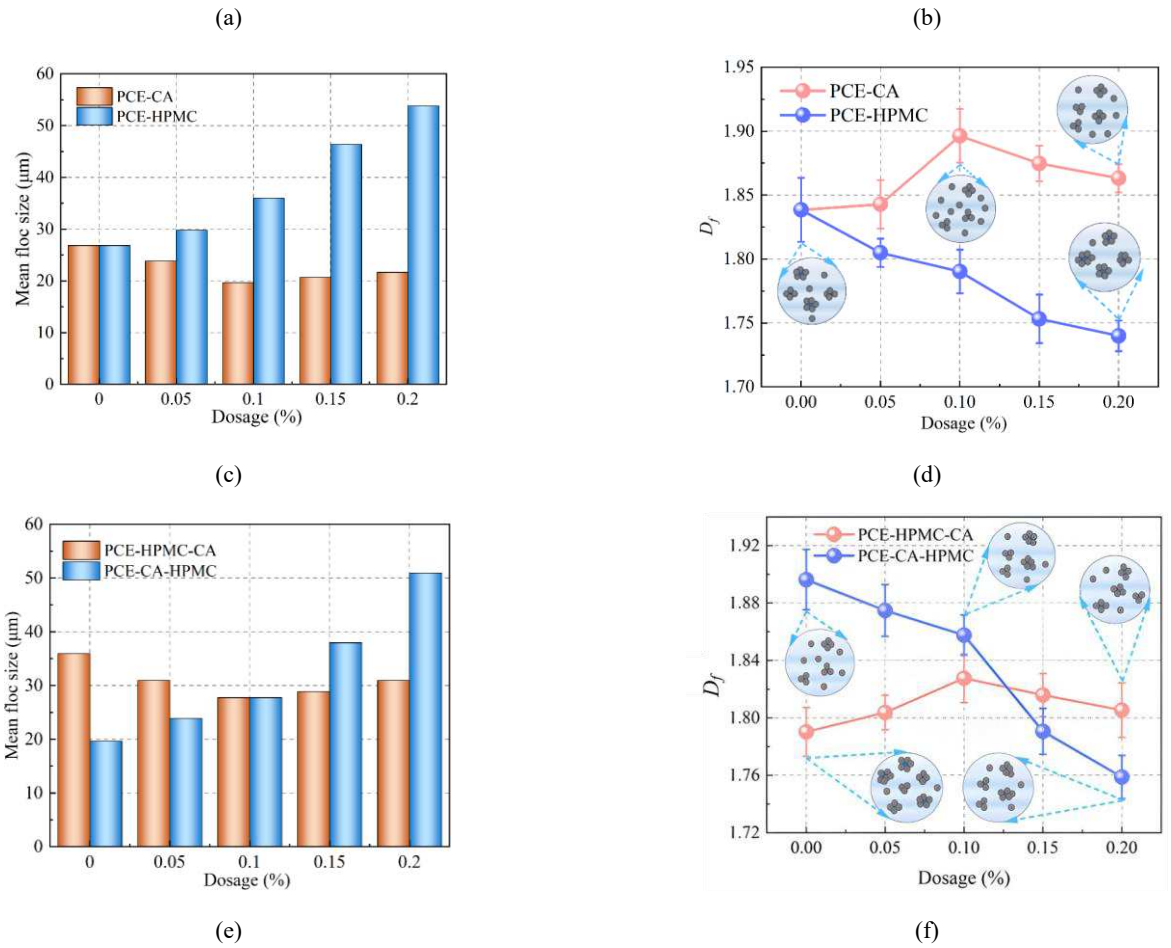


Fig. 4. Mean floc size and two-dimensional projected fractal dimension of different admixture systems: (a) PCE, mean floc size; (b) PCE, D_f; (c) PCE-CA and PCE-HPMC, mean floc size; (d) PCE-CA and PCE-HPMC, D_f; (e) PCE-HPMC-CA and PCE-CA-HPMC, mean floc size; (f) PCE-HPMC-CA and PCE-CA-HPMC, D_f.

The two ternary systems further highlight the contrasting roles of CA and HPMC. In the PCE-HPMC-CA system, with the PCE and HPMC dosages fixed at 0.60% and 0.10%, respectively, the mean floc size first decreased and then increased with increasing CA dosage, while D_f showed the opposite trend, as shown in Figs. 4(e) and (f). At a CA dosage of 0.10%, the paste exhibited a relatively small mean floc size and a relatively high D_f, together with a low-shear peak stress of 38.17 Pa. Further addition of CA increased the combined proportion of flocs in the M, L, and EL size ranges, while the low-shear peak stress increased to 90.40 Pa. The floc size distribution shown in Fig. 5(d) exhibited the same stage-dependent variation.

In the PCE-CA-HPMC system, the PCE and CA dosages were fixed at 0.60% and 0.10%, respectively. Increasing the HPMC dosage continuously increased the mean floc size and decreased D_f, as shown in Figs. 4(e) and (f). Fig. 5(e) further shows a gradual shift in the floc size distribution toward medium and large size ranges. The low-shear peak stress increased from 5.89 Pa for P-CA0.10 to 382.79 Pa for P-CA-HPMC0.20. Thus, even in the simultaneous presence of PCE and CA, HPMC continued to promote the formation of larger flocculated structures and increased the structural resistance of the paste.

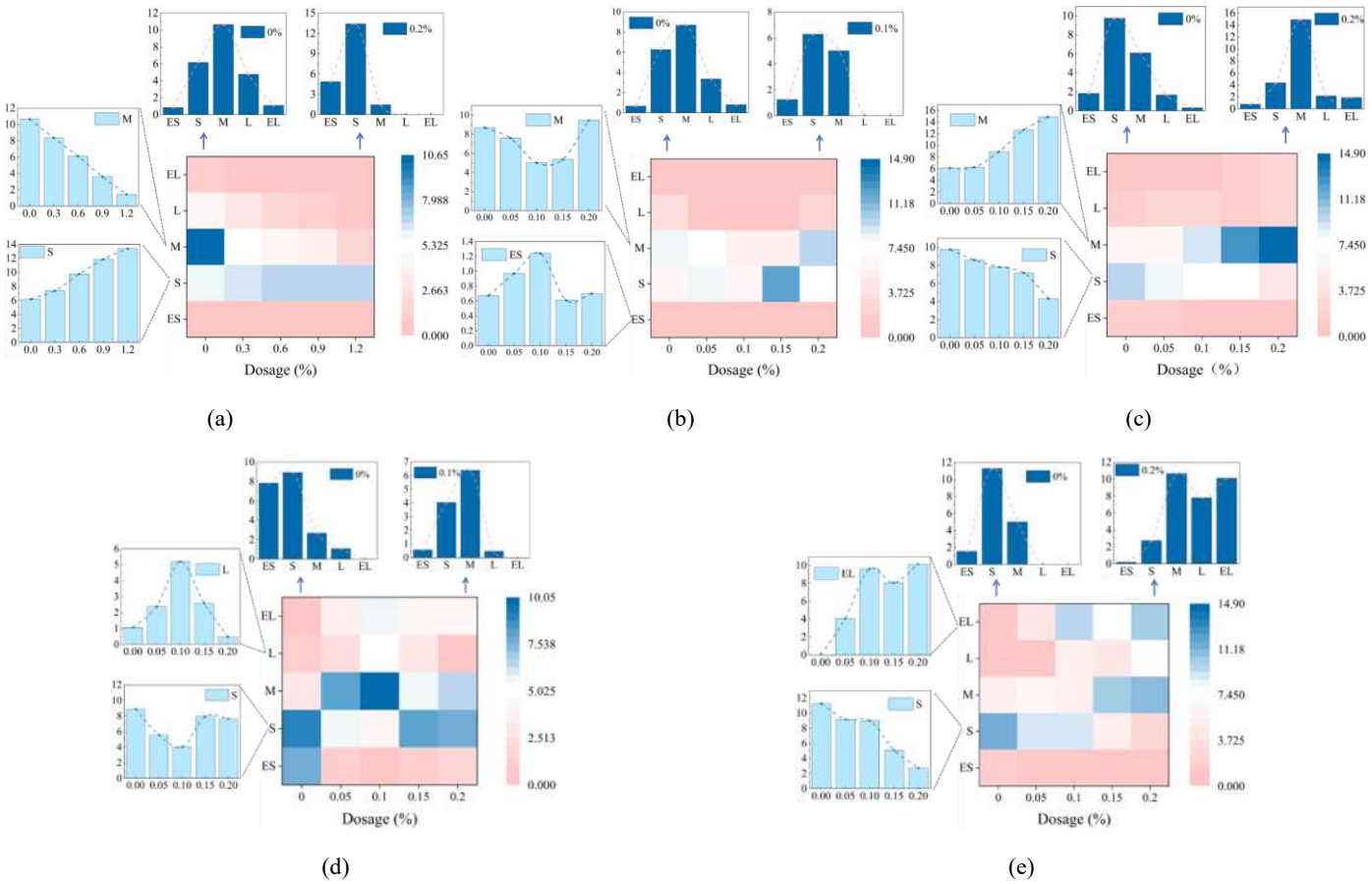


Fig. 5. Area fractions of flocs in different size ranges for different admixture systems: (a) PCE, (b) PCE-CA, (c) PCE-HPMC, (d) PCE-HPMC-CA, and (e) PCE-CA-HPMC.

3.3 Apparent ζ potential of cement particles in different admixture systems

Fig. 6 shows the variation in the apparent ζ potential of cement particles in the different admixture systems. Both admixture type and dosage markedly altered the electrokinetic state of the particle interface, and these variations showed clear correspondence with the floc structure and rheological response.

For the PCE-only system, increasing the PCE dosage shifted the apparent ζ potential continuously from +1.2 to -10.5 mV. Over the same dosage range, the mean floc size decreased, the proportion of small flocs increased, and the yield resistance of the paste was substantially reduced. Adsorbed PCE modifies the particle interfacial state, while its polyether side chains provide steric hindrance that further suppresses particle aggregation. Accordingly, the negative shift in apparent ζ potential occurred simultaneously with refinement of the floc structure.

The PCE-CA system exhibited a non-monotonic variation. With increasing CA dosage, the apparent ζ potential decreased from approximately -6.6 mV to a minimum of approximately -10.5 mV and then increased to approximately -8.9 mV. At 0.10% CA, the floc size was relatively small, the proportion of flocs in the M, L, and EL size ranges was reduced, and the low-shear peak stress reached its minimum value. Further addition of CA led to renewed coarsening of the floc structure and a corresponding increase in yield resistance. The simultaneous turning points observed in apparent ζ potential and structural parameters within a similar dosage range reflect the dosage-dependent effect of CA. This behavior may be associated with Ca^{2+} complexation and modification of the

particle interfacial state.

With increasing HPMC dosage, the apparent ζ potential of the PCE-HPMC system shifted continuously toward zero, from approximately -6.6 mV to approximately -1.6 mV at 0.20% HPMC. Meanwhile, the mean floc size and the proportion of flocs in the M, L, and EL size ranges continuously increased, D_f decreased, and the yield resistance increased substantially. Thus, the shift in apparent ζ potential toward zero coincided with increases in floc size and yield resistance. This behavior reflects the combined effects of changes in the particle interfacial state, continuous-phase thickening, and polymer-chain interactions.

In the PCE-HPMC-CA system, with the PCE and HPMC dosages fixed at 0.60% and 0.10%, respectively, the apparent ζ potential first decreased from approximately -3.4 to -6.7 mV and then increased to approximately -5.0 mV as the CA dosage increased. This trend was broadly consistent with the initial decrease and subsequent increase in both mean floc size and low-shear peak stress. Even in the presence of HPMC, CA retained a pronounced dosage-dependent effect, while its influence was also coupled with the thickening effect and structural changes associated with HPMC.

In the PCE-CA-HPMC system, with the PCE and CA dosages fixed at 0.60% and 0.10%, respectively, increasing the HPMC dosage shifted the apparent ζ potential continuously toward zero, from approximately -10.5 to -2.7 mV. Meanwhile, the mean floc size continuously increased, D_f decreased, and the low-shear peak stress increased from 5.89 to 382.79 Pa. These results indicate that increasing the HPMC dosage continued to modify the particle interfacial state in the presence of both PCE and CA and was accompanied by the formation of larger flocculated structures.

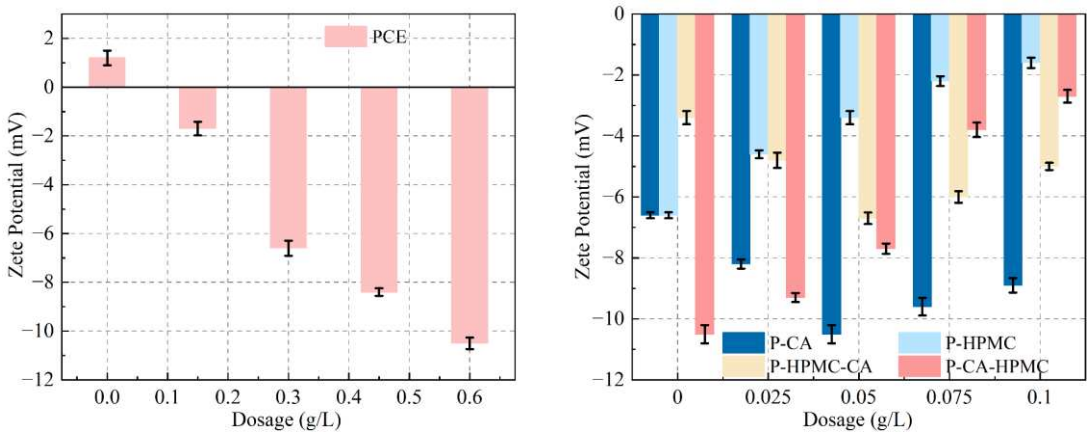


Fig. 6. Apparent ζ potential of cement particles in different admixture systems.

3.4 Residual organic carbon in blended-admixture systems

Fig. 7 compares the measured TOC values of the blended-admixture systems with the additive values obtained by summing the supernatant TOC contents of the corresponding single-admixture systems at the same concentrations. This comparison characterizes the effect of admixture coexistence on the total residual organic carbon in the aqueous phase.

In the PCE-HPMC system, both the measured and additive TOC values increased with HPMC concentration, while the measured values remained below the additive values and the difference progressively widened, as shown in Fig. 7(a). The PCE-CA system exhibited the same direction of deviation, but with a smaller difference, as shown in Fig. 7(b). Thus, combined addition produced a lower residual organic-carbon content than the additive baseline, with the magnitude depending on admixture composition.

The ternary systems also exhibited negative deviations from the additive baseline. In the PCE-HPMC-CA system, both TOC values increased with CA concentration, while the difference between them increased progressively, as shown in Fig. 7(c). In the PCE-CA-HPMC system, the additive value increased approximately linearly with HPMC concentration, whereas the measured value remained lower and the difference continued to widen, as shown in Fig. 7(d). These results show that the residual organic-carbon response remained non-additive when all three admixtures coexisted.

The variation in TOC deviation with admixture composition and concentration reflects a composition-dependent aqueous-phase response. In the HPMC-containing paste series, increasing HPMC dosage also shifted the apparent ζ potential toward zero, increased floc size, and raised flow resistance. Together, the TOC, electrokinetic, and structural measurements characterize the coupled changes accompanying admixture coexistence.

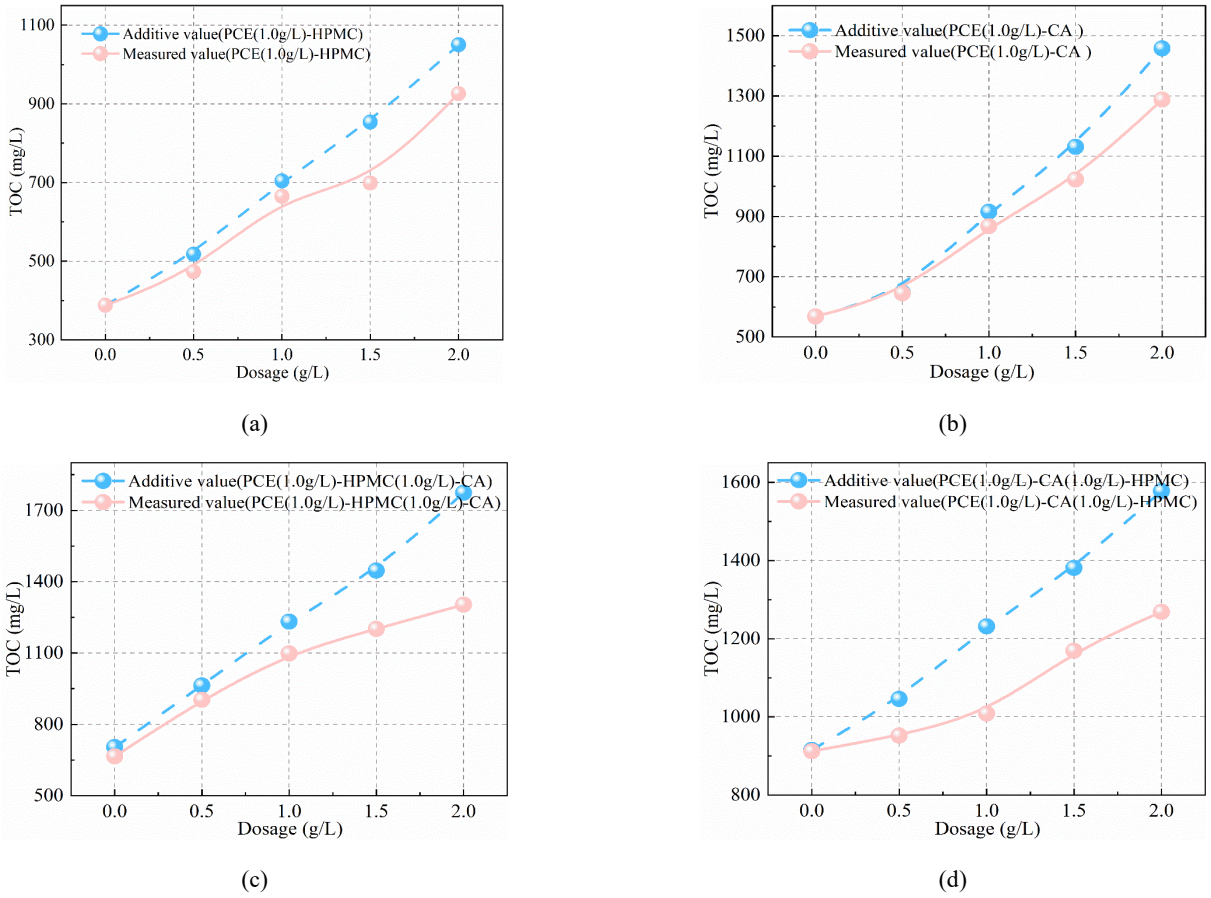


Fig. 7. Additive TOC values derived from single-admixture systems and measured TOC values of blended-admixture systems: (a) PCE-HPMC; (b) PCE-CA; (c) PCE-HPMC-CA; (d) PCE-CA-HPMC.

3.5 Relationships among interfacial electrokinetic state, floc structure, and rheological properties

Fig. 8 shows the relationship between the absolute value of the apparent ζ potential, $|\zeta|$, and the two-dimensional projected fractal dimension, D_f, for the different admixture systems. Linear regression analysis was performed separately for the PCE-only, binary, and ternary systems, and D_f increased with increasing $|\zeta|$ in all three datasets. The fitted slopes were 0.01785, 0.016607, and 0.01635 mV^{-1}, respectively, with corresponding coefficients of determination (R^2) of approximately 0.960, 0.968, and 0.978. These results indicate a strong linear correlation between the absolute value of the apparent ζ potential and the two-dimensional floc structure

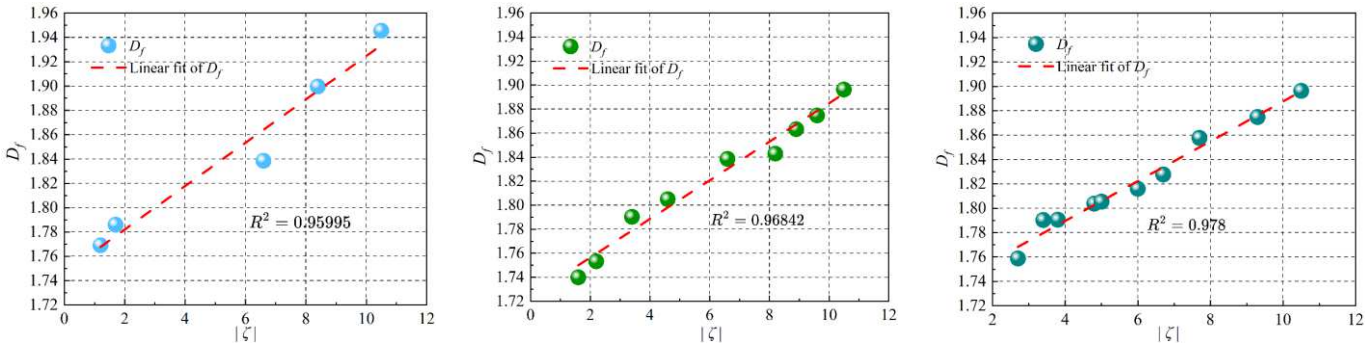
characteristics.

As shown in Fig. 9(a), the dynamic yield stress, τ_0, generally decreased with increasing D_f. In the lower-D_f range, HPMC-containing systems exhibited relatively high τ_0 values. As D_f increased, τ_0 decreased markedly for all systems. Differences among the admixture systems at similar D_f values further indicate that admixture composition affects the relationship between floc structure and yield behavior.

Fig. 9(b) shows an overall negative relationship between the consistency index, K, and D_f. At relatively low D_f, substantial differences in K were observed among the different systems, with HPMC-containing systems generally exhibiting higher values. As D_f increased, K decreased overall. Because K and n jointly define the Herschel-Bulkley flow curve, K was interpreted together with n and η_f, rather than as an independent measure of paste viscosity.

As shown in Fig. 9(c), the flow behavior index, n, generally increased with increasing D_f. Lower D_f values were primarily associated with smaller n, whereas larger D_f values corresponded to higher n. In the Herschel-Bulkley model, $n < 1$ indicates shear-thinning behavior, $n = 1$ corresponds to a linear viscous response, and $n > 1$ indicates shear-thickening behavior. Therefore, with increasing D_f, the degree of shear thinning generally decreased, and the rheological response gradually shifted toward near-linear viscous or shear-thickening behavior.

HPMC-containing systems still exhibited relatively high τ_0 and K values in the lower-D_f range, consistent with their larger floc size and higher structural resistance. The differences among the systems further show that admixture composition modulates the relationship between floc structure and rheological response.



(a) (b) (c)

Fig. 8. Relationship between the absolute value of apparent ζ potential and the two-dimensional projected fractal dimension for different admixture systems: (a) PCE; (b) PCE-CA and PCE-HPMC; (c) PCE-HPMC-CA and PCE-CA-HPMC.

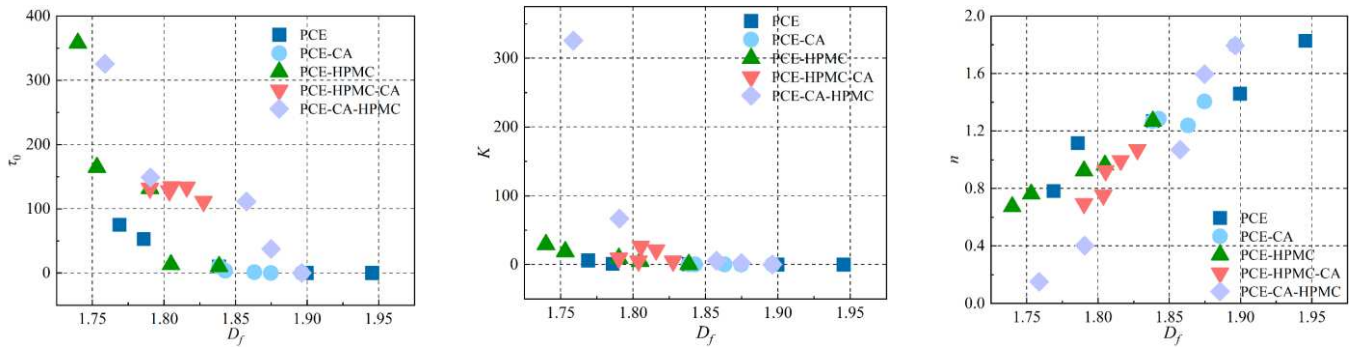


Fig. 9. Relationships between the two-dimensional projected fractal dimension and Herschel-Bulkley rheological parameters: (a) dynamic yield stress; (b) consistency index; (c) flow behavior index.

4 Conclusion

This study compared the individual and combined effects of CA and HPMC on the interfacial state, floc structure, and rheological behavior of cement pastes containing PCE. At a water-to-cement ratio of 0.29 and within the investigated admixture dosage ranges, the following conclusions were drawn:

(1) PCE promoted particle dispersion and reduced paste flow resistance. Increasing its dosage from 0 to 1.20% shifted the apparent ζ potential from +1.2 to -10.5 mV, reduced mean floc size, and increased the projected area fraction of small flocs. The low-shear peak stress decreased from 362.01 to 21.15 Pa, while the fitted dynamic yield stress decreased from 75.09 to 0 Pa. These results show consistent trends among interfacial changes, floc refinement, and reduced yield resistance.

(2) CA produced non-monotonic changes in floc structure and low-shear response. At a fixed PCE dosage of 0.60%, increasing CA dosage to 0.10% refined the flocs and reduced the low-shear peak stress to 5.89 Pa. Further addition to 0.20% coarsened the flocs and increased this stress to 12.82 Pa. With HPMC fixed at 0.10%, the stresses at the same CA dosages were 38.17 and 90.40 Pa, respectively, showing that HPMC modified the magnitude of the CA response.

(3) HPMC increased mean floc size, decreased the two-dimensional projected fractal dimension, and shifted the apparent ζ potential toward zero, accompanied by increased yield resistance. In the binary system containing PCE and HPMC, 0.20% HPMC produced a dynamic yield stress of 357.96 Pa and an apparent viscosity of 9.97 Pa·s at 100 s^{-1}. Adding 0.10% CA reduced these values to 325.71 Pa and 8.30 Pa·s, respectively. Thus, CA reduced the corresponding flow resistance while the structure-enhancing effect of HPMC persisted.

(4) Residual organic carbon in the aqueous phase exhibited non-additive behavior in the blended systems. Measured TOC in the binary system containing PCE and CA was below the sum from the corresponding individual admixture systems. The deviation was greater in the system containing PCE and HPMC and increased with HPMC concentration. Both ternary systems showed deviations in the same direction. These changes corresponded to variations in interfacial state and floc structure, reflecting interactions among the coexisting admixtures.

(5) The absolute value of the apparent ζ potential correlated strongly and linearly with the two-dimensional projected fractal

dimension. The coefficients of determination for the PCE-only, binary, and ternary systems were approximately 0.960, 0.968, and 0.978, respectively. As the fractal dimension increased, dynamic yield stress and consistency index generally decreased, whereas the flow behavior index increased. Rheological differences remained among systems with similar fractal dimensions, indicating that both floc geometry and admixture composition should be considered when interpreting paste rheology.

Data Availability Statement

The data supporting the findings of this study are available from the corresponding author upon reasonable request.

Declaration of competing interest

The authors declare that they have no known competing financial interests or personal relationships that could have appeared to influence the work reported in this paper.

Funding

The authors gratefully acknowledge the financial support from the National Natural Science Foundation of China (52478255, U21A20150, U25B20116), the Hongliu Excellent Young Talents Program of Lanzhou University of Technology, Special Project of Key Research and Development Tasks of the Autonomous Region(2025B01004-1) and Science and Technology Plan Project of Baiyin City(2024-1-30G).

References

[1] Roussel N, Bessaies-Bey H, Kawashima S, et al., Recent advances on yield stress and elasticity of fresh cement-based materials, Cem. Concr. Res., 2019, 124:105798, https://doi.org/10.1016/j.cemconres.2019.105798.

[2] Liang X, Li J, Li Z, et al., A critical review of rheological testing methods for fresh concrete, J. Build. Eng., 2025, 103:112096, https://doi.org/10.1016/j.jobe.2025.112096.

[3] Roussel N, Ovarlez G, Garrault S, et al., The origins of thixotropy of fresh cement pastes, Cem. Concr. Res., 2012, 42(1):148-157, https://doi.org/10.1016/j.cemconres.2011.09.004.

[4] Yuan Q, Zhou D, Khayat K.H., et al., On the measurement of evolution of structural build-up of cement paste with time by static yield stress test vs. small amplitude oscillatory shear test, Cem. Concr. Res., 2017, 99:183-189, https://doi.org/10.1016/j.cemconres.2017.05.014.

[5] Yoshioka K., Tazawa E.I., Kawai K., et al., Adsorption characteristics of superplasticizers on cement component minerals, Cem. Concr. Res., 2002, 32(10):1507-1513, https://doi.org/10.1016/S0008-8846(02)00782-2.

[6] Zhang Y.R., Kong X.M., Lu Z.B., et al., Effects of the charge characteristics of polycarboxylate superplasticizers on the adsorption and the retardation in cement pastes, Cem. Concr. Res., 2015, 67: 184-196, https://doi.org/10.1016/j.cemconres.2014.10.004.

[7] Lai G., Liu X., Song X., et al., A mechanistic study on the effectiveness of star-like and comb-like polycarboxylate superplasticizers in cement pastes, Cem. Concr. Res., 2024, 175: 107389, https://doi.org/10.1016/j.cemconres.2023.107389.

[8] Li R., Xue J., Wan X., et al., Influence of the anionic charge of PCE superplasticizers on the rheology of LC3 cement-A mechanistic comparison with O.P.C., Constr. Build. Mater., 2025, 486: 141979, https://doi.org/10.1016/j.conbuildmat.2025.141979.

[9] Nicia D., Jakob C., Jansen D., et al., Thixotropy of superplasticized cement pastes-Underlying mechanisms considering the polycarboxylate molecular structure, interparticle interactions and hydration kinetics, Cem. Concr. Res., 2023, 173: 107289, https://doi.org/10.1016/j.cemconres.2023.107289.

[10] Han K., Guo T., Meng F., et al., New insight into structural build-up modification by PCE superplasticizers during early C3A hydration, Cem. Concr. Res., 2026, 199: 108048, https://doi.org/10.1016/j.cemconres.2025.108048.

[11] Ma B., Peng Y., Tan H., et al., Effect of hydroxypropyl-methyl cellulose ether on rheology of cement paste plasticized by polycarboxylate superplasticizer, Constr. Build. Mater., 2018, 160: 341-350, https://doi.org/10.1016/j.conbuildmat.2017.11.010.

[12] Brumaud C., Baumann R., Schmitz M., et al., Cellulose ethers and yield stress of cement pastes, Cem. Concr. Res., 2014, 55: 14-21, https://doi.org/10.1016/j.cemconres.2013.06.013.

[13] Ma S., Qian Y., Kawashima S., Experimental and modeling study on the non-linear structural build-up of fresh cement pastes incorporating viscosity modifying admixtures, Cem. Concr. Res., 2018, 108: 1-9, https://doi.org/10.1016/j.cemconres.2018.02.022.

[14] Chen W., Zhou Y., Yu Q., et al., Microscopic thickening mechanisms of hydroxypropyl methyl cellulose ether anti-washout admixture and its impact on cementitious material rheology and anti-dispersal performance, J. Build. Eng., 2024, 89: 109346, https://doi.org/10.1016/j.jobe.2024.109346.

[15] Sun Z., Chen C., Xu B., et al., Influence of HPMC chain length on rheological properties of cement paste, J. Build. Eng., 2026, 130: 117060, https://doi.org/10.1016/j.jobe.2026.117060.

[16] Pourchez J., Peschard A., Grosseau P., et al., HPMC and HEMC influence on cement hydration, Cem. Concr. Res., 2006, 36(2):288-294, https://doi.org/10.1016/j.cemconres.2005.08.003.

[17] Yao X., Zhou D., Zhang H., et al., Effects of polycarboxylate superplasticizer and hydroxypropyl methylcellulose on the properties of ferric-rich sulfoaluminate cement, Constr. Build. Mater., 2024, 425: 136064, https://doi.org/10.1016/j.conbuildmat.2024.136064.

[18] Möschner G., Lothenbach B., Figi R., et al., Influence of citric acid on the hydration of Portland cement, Cem. Concr. Res., 2009, 39(4):275-282, https://doi.org/10.1016/j.cemconres.2009.01.005.

[19] Liu Y., Zhang Z., Jing R., et al., The interaction of sodium citrate and polycarboxylate-based superplasticizer on the rheological properties and viscoelasticity of cement-based materials, Constr. Build. Mater., 2021, 293: 123466, https://doi.org/10.1016/j.conbuildmat.2021.123466.

[20] Li H., Lu Z., You Z., et al., Further understanding of hydration and setting performance of cement with citrate retarders: Effects of sulfate carriers and cations, Constr. Build. Mater., 2025, 492: 142844, https://doi.org/10.1016/j.conbuildmat.2025.142844.

[21] Plank J., Winter C., Competitive adsorption between superplasticizer and retarder molecules on mineral binder surface, Cem. Concr. Res., 2008, 38(5):599-605, https://doi.org/10.1016/j.cemconres.2007.12.003.

[22] Bessaies-Bey H., Hot J., Baumann R., et al., Consequences of competitive adsorption between polymers on the rheological behaviour of cement pastes, Cem. Concr. Compos., 2014, 54: 17-20, https://doi.org/10.1016/j.cemconcomp.2014.05.002.

[23] Teng L., Wei J., Khayat K.H., et al., Effect of competitive adsorption between specialty admixtures and superplasticizer on structural build-up and hardened property of mortar phase of ultra-high-performance concrete, Cem. Concr. Compos., 2023, 141: 105130, https://doi.org/10.1016/j.cemconcomp.2023.105130.

[24] Mostafa A.M., Yahia A., New approach to assess build-up of cement-based suspensions, Cem. Concr. Res., 2016, 85: 174-182, https://doi.org/10.1016/j.cemconres.2016.03.005.

[25] Zhang Z., Jia Z., Shi J., et al., Clarifying and quantifying the driving force for the evolution of static yield stress of cement pastes, Cem. Concr. Res., 2023, 167: 107129, https://doi.org/10.1016/j.cemconres.2023.107129.

[26] Zhang K., Mezhov A., Schmidt W., et al., Chemical and thixotropic contribution to the structural build-up of cementitious materials, Constr. Build. Mater., 2022, 345: 128307, https://doi.org/10.1016/j.conbuildmat.2022.128307.

[27] Han K., Guo T., Shu X., et al., Structural build-up of cement pastes-Underlying mechanisms considering the particle packing, colloidal interactions and hydration kinetics, Constr. Build. Mater., 2024, 438: 137030, https://doi.org/10.1016/j.conbuildmat.2024.137030.

[28] Ye H., Zhang J., Gao X., et al., Showing the role of weakly-bound particles flocculation in the reversibility of thixotropic behavior for fresh cement paste, Constr. Build. Mater., 2024, 411: 134624, https://doi.org/10.1016/j.conbuildmat.2023.134624.

[29] Song H., Lu Y., Dong H., et al., Experimental study on the effect of mixing parameters on the rheological behaviour and micro-flocculation structure of ultrafine Portland cement slurry, Constr. Build. Mater., 2024, 449: 138526, https://doi.org/10.1016/j.conbuildmat.2024.138526.

[30] Zhang C., Liu R., Chen M., et al., Influence of the flocculation effect on the rheological properties of cement slurry, Powder Technol., 2022, 398: 117118, https://doi.org/10.1016/j.powtec.2022.117118.

[31] Zhang Y., Kong X., Gao L., et al., Characterization of the mesostructural organization of cement particles in fresh cement paste, Constr. Build. Mater., 2016, 124: 1038-1050, https://doi.org/10.1016/j.conbuildmat.2016.08.143.

[32] Chen Z., Zhao G., Chen B., et al., Influence of flocculation structure on time-dependent fluidity and rheological property of cement paste: Analytical models based on fractal theory, Constr. Build. Mater., 2024, 455: 139137, https://doi.org/10.1016/j.conbuildmat.2024.139137.

[33] Zingg A., Winnefeld F., Holzer L., et al., Adsorption of polyelectrolytes and its influence on the rheology, zeta potential, and

microstructure of various cement and hydrate phases, J. Colloid Interface Sci., 2008, 323(2):301-312, https://doi.org/10.1016/j.jcis.2008.04.052.

[34] Qian R., Zhang Y., Zhang Y., et al., Effects of aqueous-phase speciation on Portland cement and supplementary cementitious materials as reflected using zeta potential of powder suspensions, Constr. Build. Mater., 2022, 345: 128258, https://doi.org/10.1016/j.conbuildmat.2022.128258.

[35] Real S., Bowen P., Moreno R., et al., Impact of pore solution composition and superplasticizers on the interparticle forces and rheology of metakaolin suspensions, Cem. Concr. Res., 2025, 195: 107901, https://doi.org/10.1016/j.cemconres.2025.107901.

[36] Martins J.R., Rocha J.C., Novais R.M., et al., Zeta potential in cementitious systems: A comprehensive overview of influencing factors and implications on material properties, J. Build. Eng., 2025, 99: 111556, https://doi.org/10.1016/j.jobe.2024.111556.

[37] Sun H., Teng L., Yu X., et al., How does competitive adsorption between VMA and PCE influence yield stress of cement paste? A novel insight from interparticle forces and percolation threshold, Cem. Concr. Res., 2026, 205: 108233, https://doi.org/10.1016/j.cemconres.2026.108233.